Textured Microcapsules through Crystallization

Samuel R. Wilson-Whitford,[‡,†] Ross W. Jaggers,[‡] Brooke W. Longbottom,[‡,§] Matt K. Donald,[‡] Guy J. Clarkson,[‡] and Stefan A. F. Bon.[‡,]*

‡Samuel R. Wilson-Whitford, Ross W. Jaggers, Brooke W. Longbottom, Matt K. Donald, Guy J. Clarkson, and Stefan, A. F. Bon, Department of Chemistry, University of Warwick, Gibbet Hill Road, Coventry, CV4 7AL, United Kingdom.

†Samuel R. Wilson-Whitford, Department of Chemical and Biomolecular Engineering, Lehigh University, 19 Memorial Drive W., Bethlehem, Pennsylvania, 18015-3027, USA.

§Brooke W. Longbottom, Department of Chemistry, University of Cambridge, Lensfied Road, Cambridge, CB2 1EW, United Kingdom.

*Stefan A. F. Bon, E-Mail: s.bon@warwick.ac.uk

KEYWORDS Droplets, Microcapsules, Crystallization, Interfacial, Roughness, Deposition

ABSTRACT

This work demonstrates the fabrication of surface textured microcapsules formed from emulsion droplets which are stabilized by an interlocking mesh of needle-like crystals. Crystals of the small organic compound decane-1,10-bis(cyclohexyl carbamate) are formed within the geometric

confinement of the droplets, through precipitation from a binary-solvent dispersed phase. This binary mixture consists of a volatile solvent and non-volatile carrier oil. Crystallization is facilitated upon supersaturation due to evaporation of the volatile solvent. Microcapsule diameter can be easily tuned using microfluidics. This approach also proves to be scalable when using conventional mixers, yielding spikey microcapsules with diameters in the range of 10-50 μm. It is highlighted that the capsule shape can be molded and arrested by jamming using recrystallization in geometric confinement. Moreover, it is show that these textured microcapsules show a promising enhanced deposition onto a range of fabric fibers.

INTRODUCTION

Microcapsules are being used as storage and delivery systems for active ingredients in a widespread range of commercial applications including cosmetics,[1–4] healthcare,[5–7] agriculture,[8,9] biological mimics,[10–13] etc. They can have a variety of designs, the simplest form being a single internal liquid-based core surrounded by a solid shell. The chemical and physical characteristics of this shell influence the colloidal stability of capsules in formulations, dictate the permeability and mechanical robustness of the capsules, and can potentially regulate substrate adhesion.

In this work we would like to address the feature of crystallinity of the capsule wall, with a focus on the fabrication of microcapsules of which the capsule wall is composed of an inter-locked mesh of needle-like crystals, which besides capsule rigidity and semi-permeability, provides a roughened surface texture. The latter, as we will see, will show promising results for capsule deposition on fibrous substrates.

By no means do we claim that the idea of fabrication of capsules with a (semi-)crystalline shell is new, nor that through crystallinity we can regulate capsule robustness or permeability. For

example, the concept of polymer microcapsules made through coacervation or interfacial polymerization with a semi-crystalline shell goes back to Chang in 1964.[14] Pioneering work by Fessi and coworkers in the late 1980s showed the fabrication of poly(D,L-lactic acid) and other semi-crystalline nano-sized capsules through interfacial polymer deposition.[15,16] Suresh and coworkers, in the mid 1990s, reported a strong influence (order of magnitude) on capsule permeability as a result of crystallinity in polyurea microcapsules.[17] More recently, elegant work by Li and coworkers demonstrated that poly(L-lactic acid) (PLLA) deposition on the interface of mini-emulsion droplets resulted in the formation of crystalline capsules with bent lamellae sheets of PLLA.[18] In further work they showed that amphiphilic block copolymers which had the ability to crystallize at the emulsion droplet interface could be used to fabricate nanocapsules with a crystalline shell.[19] Li and coworkers coined their structures "crystalsomes" in analogy to "colloidosomes", the latter being microcapsule architectures in which the shell is built from colloidal particles, as pioneered by Velev and Dinsmore.[20,21]

For colloidosomes, emulsion droplets are decorated with an armored layer of solid particles. These particles adhere to the interface in a phenomenon known as Pickering stabilization.[22–24] Velev and Dinsmore reinforced their structures to improve robustness of the semi-permeable capsule walls, through physi/chemisorptive crosslinking with casein and/or glutaraldehyde, and partial autohesion of the polystyrene colloidal building blocks, respectively. Various other reinforcement or scaffolding approaches have been reported, including electrodeposition,[25] 2D colloidal crystal formation,[26,27] building a shell supporting scaffold through polymerization,[8,28,29] and gelation of the emulsion droplet template.[30]

A different strategy to provide colloidosome capsules with rigidity is through jamming of the colloidal building blocks.[31] This allows for the fabrication of non-spherical emulsion droplets.[32]

The structural rigidity can be further enhanced if the colloidal building blocks can interlock. The use of rod-like or needle-like colloids makes this viable.

Paunov used polymeric, epoxy microrods to stabilize the droplet surface in a water (1.5 % agarose gel)-in-oil emulsion.[30,33–35] Rods were found to sit at the gelled droplet interface which remained stable when transferred from an oil to a water continuous phase. Stoyanov demonstrated the use of calcium carbonate ($CaCO_3$) rods to stabilize air bubbles. [36] It was found that the stabilized bubbles had a bimodal distribution based on how crystalline rods sat at the interface. The capsules had very high stiffness as a result of $CaCO_3$ crystal interlocking, a phenomenon also observe by Zhu.[37]

A practical downside of using solid particles as building blocks to fabricate supracolloidal microcapsules through emulsion droplet templating is that often emulsification strategies are not compatible. Microfluidic devices,[31,38] membrane emulsifiers, and shear homogenizers, are easily fouled or clogged up with particle coagulum at high shear regimes. In addition, solid particles can be abrasive, with detrimental consequences for the emulsification equipment.

The solution we demonstrate here is to generate a layer of interlocking needle-like colloidal building blocks *in situ* at the interface from the inside of the droplets, after the emulsification step has taken place. Inspired by the micro-drop concentrating (MDC) principle,[39] and the works on (semi-)crystalline polymer capsules and crystalsomes mentioned above, we demonstrate that a supersaturation point can be used to nucleate and grow a textured multi-crystalline shell from inside a droplet containing a carrier oil and an organic crystallizable small molecular building block. For this fabrication of the surface textured microcapsules, a compound with the minutest aqueous solubility should be used in order to prevent structural degradation from shell-crystal ripening. Examples of micro-drop concentrating (MDC) have involved microfluidic devices,

suggesting a microfluidic approach could be taken to develop a model system for organic crystal, droplet stabilization. Commonly, MDC, is used to grow single crystals under specific controlled environments. Evaporation times or solvent diffusion occur over prolonged time scale promoting droplet confined single crystal nucleation and growth.[40–42] In other words, the objective in MDC is to minimize the occurrence of nucleation events in each droplet. In our study we purposely decrease the overall timescale of crystallization, so to trigger many interfacial crystal nucleation events. A benefit of our approach which builds an inter-locked mesh of crystalline colloidal building blocks *in situ* in comparison to using the Pickering stabilization approach of pre-made colloidal particles, is that fouling and jamming of microfluidic set-ups is prevented, as supersaturation and crystallization sets in downstream. Our microcapsule formation route differs from the crystalsome approach taken by Li and coworkers,[18,19] in that we purposefully trigger a multitude of nucleation events to produce microcapsules with a textured shell composed of scores of crystals. We will demonstrate that these spiky capsules show improved adhesion to fabrics, compared to their smooth counterparts.

MATERIALS AND METHODS

Materials: Cyclohexyl isocyanate (98%), decanediol (98%), Nile Red, dibutyltin dilaurate (95%), 1,6-hexandiol diacrylate (80%), phenylbis(2,4,6-trimethyl-benzoyl)phospine oxide (97%), Isophorone diisocyanate (98%), diethylene triamine (99%), dichloromethane and Mowiol 8-88 $M_w \approx 67000$ g mol^{-1} were purchased from Sigma-Aldrich. *n*-Dodecane (99%) was purchased from VWR and *n*-decanol (98%) was purchased from Alfa Aesar. Anhydrous chloroform (>99.9%) was purchased from Acros Organics.

Equipment: (Crystallography) Xcalibur Gemini diffractometer with Ruby CCD area detector, (NMR) Ascend™-400, (IR) Bruker Alpha FTIR, (HRMS) Bruker maXis™, (DSC) Mettler-Toledo DSC I STARe, (Light microscopy) Olympus IX73 inverted microscope with Andor Zyla 4.4 plus sCMOS and Leica DM2500M (Confocal microscopy) Leica DMI6000 using a HC PL FLUOTAR 10.0x 0.30 dry objective lens, at a scan speed of 8000 Hz, (SEM) Zeiss Gemini SEM 500 at 0.5 kV with carbon coating (Rotary oven) SciGene Model 777 Microarray oven.

Decane-1,10-bis(cyclohexyl carbamate) (DBCC) synthesis: Decanediol (2.000 g, 11.48 mmol, 1.0 eq.) was dissolved in dry chloroform at 45 °C under $N_{2(g)}$. To this, cyclohexyl isocyanate (2.945 g, 23.53 mmol, 2.05 eq.) was added followed by dibutyltin dilaurate (0.145 g, 0.23 mmol, 0.02 eq.). The reaction was stirred for 3 hr during which a white precipitate was formed. The precipitate was filtered and washed with chloroform three times and dried under vacuum, yielding a white crystalline powder (4.778 g, 11.25 mmol, 97.9 %).

Example synthesis microfluidic capsules: A continuous phase contained 5 w/w % of PVA (Mowiol 8-88 M_w 67000 g mol^{-1}) was used at a flow rate of 0.15 mL min^{-1}. A dispersed phase of a 9:1:0.1 by mass of DCM:dodecane:DBCC was used at 0.02 mL min^{-1}. Droplets were delivered to a vial of water and left undisturbed. DCM evaporated from the droplets until a supersaturation was reached and DBCC crystallization occurred, forming crystal stabilized organic capsules of diameter ≈195 μm.

Synthesis small spikey capsules: A continuous phase of 2 w/w % of PVA (Mowiol 8-88 M_w 67000 g mol^{-1}) was prepared. 9.00 g of solution was heated to 32 °C with constant stirring at 1000 rpm in crimp vial. Separately a dispersed phase of DCM:dodecane:DBCC, 9:1:0.1 by mass, was prepared. 1.00 g of dispersed phase was added via pipette to vial and was left to stir for 30 min. As DCM evaporated the suspension became whiter as capsules formed.

Synthesis small smooth capsules: Continuous phase preparation is analogous to small spikey capsules. A dispersed phase of DCM:dodecane:isophorone diisocyanate, 9:1:0.1 by mass, was prepared. 1.00 g of dispersed phase was added via pipette to the open crimp vial and was left to stir for 30 min to evaporate DCM and reach the final capsule size. 250 μL of 10 wt.% diethylene triamine solution was added dropwise, leading to the smooth capsules with comparable surface chemistry.

Fiber dipping: 40 mm lengths of polyamide, polyester and cotton fibers were prepared and fitted with 0.06 g lead weights. 1 wt.% dispersions of (i) smooth and (ii) spikey microcapsules were prepared from gently centrifuged, cleaned capsules. Fibers dipped in capsule suspensions and dried overnight. Adhered capsules were counted with back-scattered light microscopy. Experiments repeated in quadruplicate.

Fabric dipping: 30x 100 mm^2 squares of cotton fabric were prepared. 1 wt.% dispersions of (i) smooth and (ii) spikey microcapsules were also prepared from centrifuged, cleaned capsules. Samples were dipped in suspensions (15 each) and air dried overnight. Adhered capsules were counted in backscattering light microscopy in sections of 1 mm^2. The fabric squares were then added to 0.1 wt.% washing detergent solution and tumbled in a rotary oven at 40 ^oC and 80 rpm overnight. Samples were dried and adhered capsules were recounted.

RESULTS AND DISCUSSION

The primary organic molecular building block for our textured capsule walls is the hydrogen bonding organic molecule decane-1,10-bis(cyclohexyl carbamate) (DBCC), which forms an organogel in organic solvents (such as dodecane) from concentrations of ≥ 1 w/w%. Synthetic

details of DBCC are outlined in the experimental section and the supplementary information (S1-S3).

As is the norm for organogelators, DBCC remains insoluble in its chosen solvents at room temperature, but dissolves at elevated temperatures (see DSC data (S4)). Upon cooling, DBCC crystallizes, trapping organic solvent as a result of the crystal jamming of needle like crystals. The resulting organogels are shown by microscopy (S5).

These interesting, jammed structures led to the question: *What will occur if we trigger supersaturation and confine crystallization in a template droplet?* It was hypothesized that confinement, in an oil-*in*-water emulsion droplet, would result in either one large crystals protruding into the aqueous phase, or an interlocked mesh of smaller crystals that would stabilize the droplet surface, much like a capsule shell. Due to synthetic challenges, a microfluidic approach was adopted to better control the initial droplet size distribution (Figure 1).

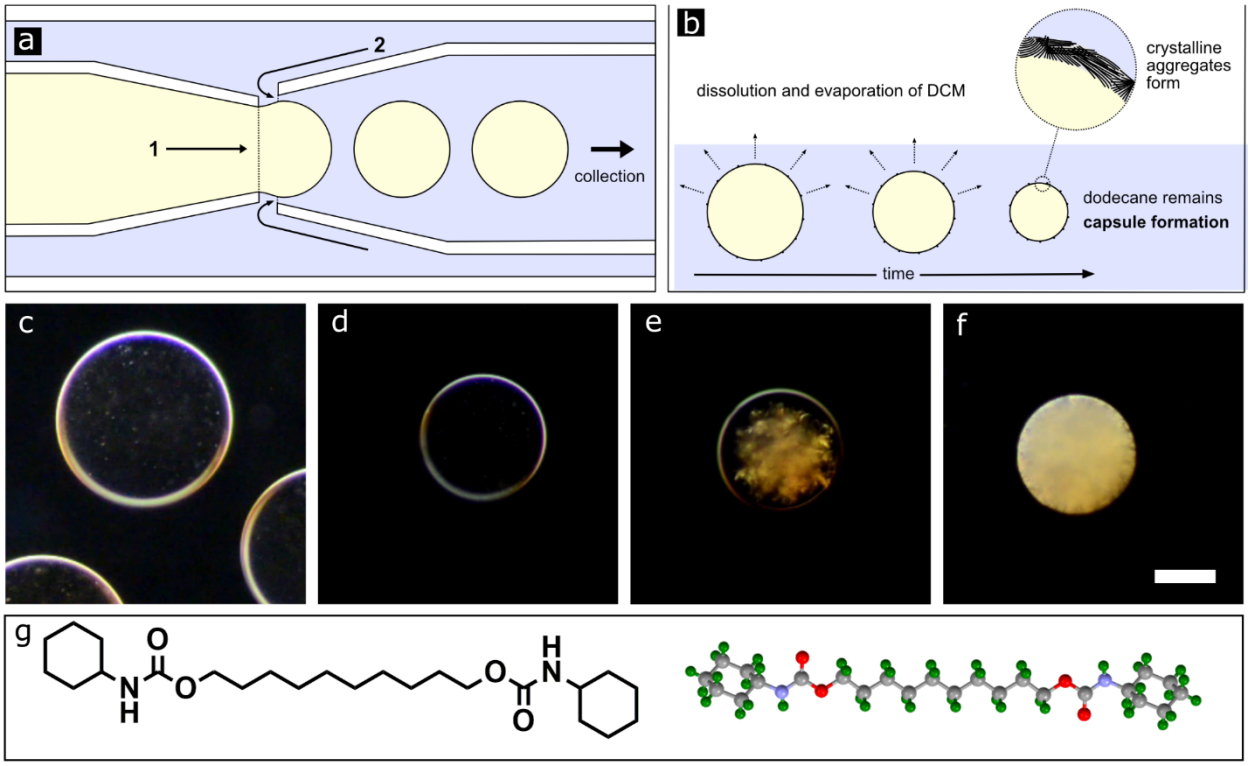

Figure 1. *(a)* Schematic of the formation of organic droplets from a microfluidic device. Organic solution, 1, containing DCM, DBCC and dodecane, meets an aqueous flow, 2, of PVA solution to form droplets *(b)* Following droplet formation, DCM dissolves into the aqueous phase and evaporates at the air-water interface. Total DCM evaporation causes DBCC crystallization, forming an armor around the droplet *(c)* Droplet immediately following its formation *(d)* 7 min 27 s, total DCM evaporation *(e)* 7 min 31 s, DBCC supersaturation *(f)* 7 min 34 s, completed capsule. Scale bar = 100 μm *(g)* structural image and crystallographic model of DBCC.

A binary solvent system of dichloromethane (DCM), as a volatile co-solvent, and dodecane as carrier oil was proposed as the dispersed phase. After droplet formation, DCM subsequently evaporates by diffusion through the continuous phase, unlike the less volatile dodecane component of the dispersed phase. As the total volume of DCM in the dispersed droplets decreases, the solubility of DBCC in the droplet is reduced. At a critical saturation point, the crystallization of DBCC will spontaneously occur to produce droplets of dodecane containing the crystalline material, stabilizing the oil-water interface.

A flow-focusing microfluidic device (S6) is used to prepare stabilized oil-in-water droplets of low size dispersity (Figure 1a-1b). A 5 w/w % PVA (M_w 67 kg·mol^{-1}) solution is used as the aqueous phase, [43] to stabilize droplets in solution as well as increase the continuous phase viscosity to aid droplet generation. The dispersed phase of DCM:dodecane:DBCC meets this aqueous phase at the flow-focusing junction to produce oil-in-water droplets. Typical flow rates for the aqueous and organic phases were 0.15 and 0.02 mL·min^{-1}, respectively.

Figure 1c shows DCM:dodecane:DBCC droplets (9:1:0.1 by mass), immediately after leaving the microfluidic device via a 100 mm outlet tube, and have a diameter of 281 μm. Tiny particles nucleate and adhere to the interface, this is indicated by the non-Brownian trajectory of these

primary particles as they move along the droplet surface (Video V1). These crystals form as a result of supersaturation at the interface where the DCM concentration is in evaporative flux. In Figure 1d-1f and the supporting Video V1, the diameter of the droplet is seen to reduce over time and it begins to rise through the continuous phase indicating a reduction in density due to loss of DCM relative to dodecane. Primary interfacial particles can be seen to increase in size by a small amount over the duration of droplet shrinkage. Once the droplet approaches its final size of *ca*. 193 μm, a crystalline shell spontaneously forms. The shell is seen to rapidly form across the surface of the droplet until it is completely covered, appearing to nucleate at the droplet surface. A localized concentration of DBCC at the interface, along with the preference of crystals to remain at the interface, promotes nucleation at multiple points on the droplet surface, forming a shell of multiple small crystals and not a large single crystal shell.[44] Light and electron microscopy of organogels (S5) and capsules (S8 and S13a) suggest that the final shell structure is formed from jammed crystals, and not by traditional Pickering stabilization.

To probe whether these droplets are indeed encapsulated by a jammed layer of crystallized DBCC, the microcapsules were examined using confocal microscopy. Droplets were loaded with Nile Red (λ_{ex} = 550 nm; λ_{em} = 630 nm) at a concentration of 2 mg·ml^{-1} prior to capsule formation to provide a fluorescent label. The DCM:dodecane ratio was held at 9:1 and the relative concentration of DBCC held at 10 w/w %, with respect to dodecane.

Observations of the crystal stabilized droplets (or microcapsules) at an excitation wavelength of 495 nm show that the droplets contain the dye, and that none is present in the continuous aqueous phase (Figure 2a-2b). By monitoring the emitted light at the same wavelength as the excitation, reflected light from objects which scatter, namely the crystals present on the droplet interfaces, can be observed. Here it can be seen that the surface material is clearly crystalline and rough in

topography. It is worth noting that occasionally, if a generated droplet contains an unexpected particulate defect (fouling), this can trigger DBCC nucleation and growth into a single large crystal. The formation of additional crystals at the interface is energetically less favorable than continued crystal growth of the crystal formed by the defect triggered event. The bright red, deformed object in Figure 2a is an example of this and is a droplet in which a large crystal has formed, much like in microdroplet crystallization (MDC). A bright-field microscope image has been included in the supplementary information to show this kind of crystal containing droplet more clearly (S10). The subsequent deformation of the droplet is a result of wetting to the crystal. This is similar to the use of "foreign particulates" in the research field of emulsion nucleation.[41,45]

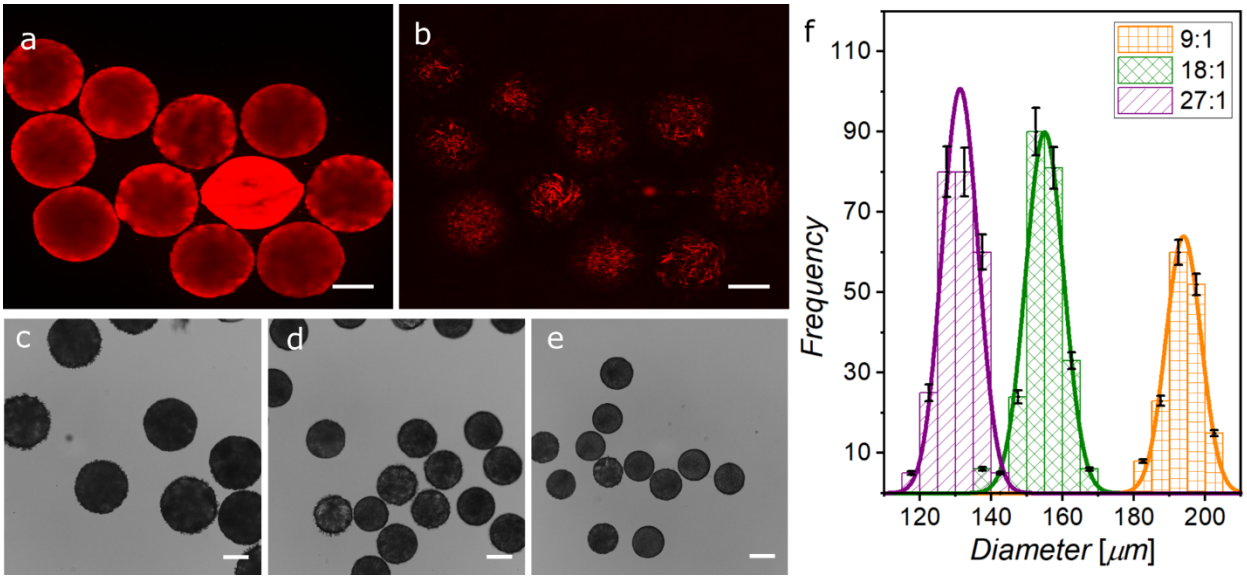

Figure 2. *(a)* Confocal microscopy of Nile red loaded DBCC capsules at fluorescence wavelength *ca*. 630 nm *(b)* Confocal microscopy of Nile red loaded DBCC capsules in reflectance mode *ca*. 495 nm. Scale bar = 100 μm. *(c)* Light microscopy of DBCC microcapsules synthesized from 9:1 *(d)* 18:1 and *(e)* 27:1 DCM:dodecane ratios *(f)* Histograms of capsule size distributions from ~200 microcapsules synthesized from 9:1 (cross normal: coral) 18:1 (cross diag.: green) and 27:1 (diag. up: purple) DCM:Dodecane ratios. Scale bar = 100 μm.

An advantage of a binary solvent system is control of the capsule size. The ratio of DCM to non-volatile organic solvent in the droplets, determines the final capsule size. This is based on the assumption that 100% of the DCM evaporates and 100% of the dodecane mass is conserved. The accuracy of this assumption was validated by preparing 3 solvent mixtures of DCM:dodecane (9:1, 18:1, 27:1). In each case the relative concentration of DBCC in dodecane was kept at 10 w/w %.

Firstly, a microscope image capturing the droplet size immediately after its generation gives an average diameter at t_0 (*e.g.* 350 μm for a 9:1 solvent mix). By using measured solvent densities at t_0 and t_∞, assuming that t_0 is 100 % the 9:1 solvent mix (1.22 g cm^{-3} – S7) and t_∞ is 100% dodecane (0.75 g cm^{-3}), a final theoretical capsule size can be inferred and compared to the measured size. In the case of the 9:1 solvent system, the predicted capsule size and the measured average capsule size were 191 μm and 193.85 ± 4.92 μm, respectively. The process was repeated for both the 18:1 (155_{theo}/154.91 ± 5.32 μm) and 27:1 (137_{theo}/131.20 ± 5.04 μm) solvent systems (Figure 2c-f and S7). This proves that (i) it is possible to control capsule size based on initial solvent mixtures and (ii) the majority of the DCM has left the droplet upon capsule formation.

Weitz,[46,47] amongst others,[48] discussed the transition between dripping and jetting regimes in microfluidic droplet generation. The mode of droplet formation can be understood by evaluating the capillary, *Ca*, and Weber numbers, *We*. Increasing the flow rates of either phase will transition the regime from dripping to jetting, which will also influence droplet size. In our system, flow rates are controlled to keep droplet generation in the dripping regime. Nonetheless, the relative flow rates of the dispersed and continuous phases within the dripping regime still determine the initial droplet size and thus the final capsule size.[49] The flow rates were kept the same for each composition (9:1, 18:1, 27:1), and we observed similar droplet diameters upon droplet generation,

indicating that variations in interfacial tension and viscosity as a result of difference in chemical composition of the droplets, were marginal.

If as proposed, primary crystals are adhering to the interface and crystallizing upon supersaturation, a smaller capsule volume will have less DBCC relative to the surface area. As a result, crystals should be smaller. Confirmation of the reduction in crystal size was found by measuring the normalized radial roughness from the center of mass of microcapsules of different sizes. The data in Figure 3a shows the reduction in surface roughness with the reduction in capsule radius. This agrees with the idea that capsule shells would be made from increasingly small crystals when decreasing the final capsule diameter. Removing the y-offset of the profiles in Figure 3a relative to the average radius of the capsule, r_{avg}, can be performed and represented as a gaussian of r-r_{avg} (Figure 3b). This shows the frequency of larger magnitude deviations from the mean radius. This is again indicative of a reduction in crystal sizes in the shell. Finally, normalizing for the radius as $(r\text{-}r_{avg})/r_{avg}$ (Figure 3c) shows the unitless comparison of surface roughness, the arithmetic mean deviation of which gives a relative roughness R_a of 2.8 $\times 10^{-2}$, 9.1 $\times 10^{-3}$, 7.6 $\times 10^{-3}$, 1.4 $\times 10^{-3}$ and 7.0 $\times 10^{-4}$ in order of decreasing capsule size. All three interpretations support an interfacial nucleation event.

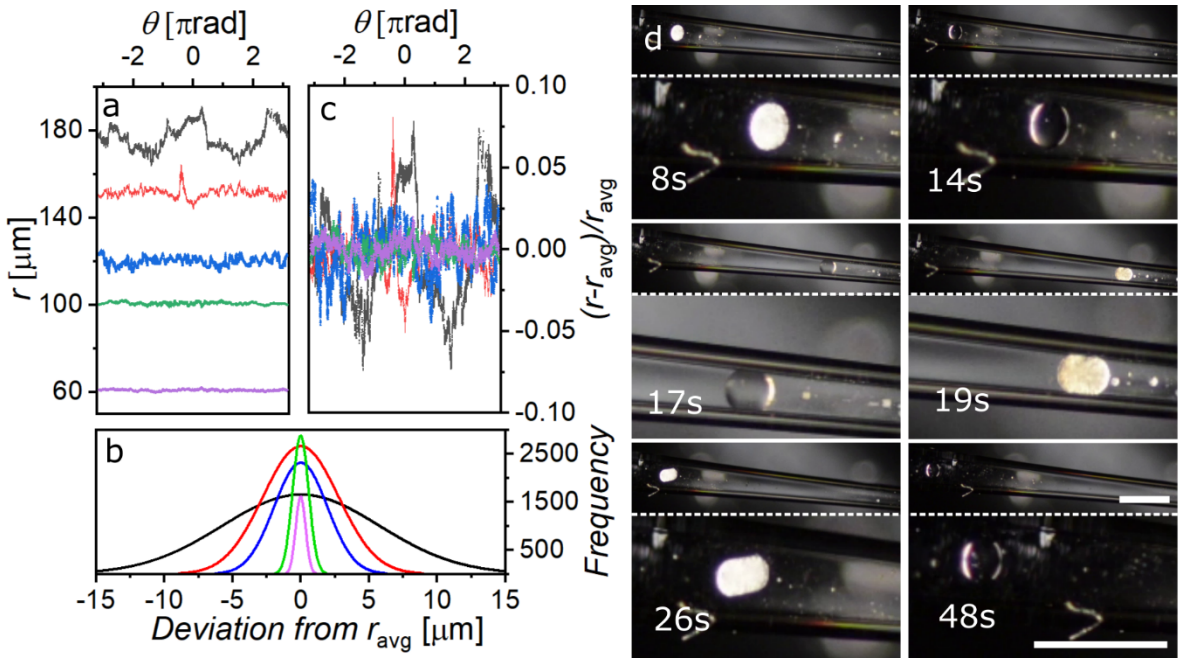

Figure 3. *(a)* Radial surface roughness profiles and *(b)* Gaussian distributions of deviation from the mean radius, in the form $r\text{-}r_{avg}$, and *(c)* radius normalized, radial surface profiles ($r\text{-}r_{avg}/r_{avg}$) of microcapsules with average radii of 177 μm (black) 152 μm (red) 120 μm (blue) 101 μm (green) 61 μm (purple) *(d)* Time-stamped images of supplementary Video V2 showing thermal dissolution and reshaping of microcapsule, into a sphereocylinder, in a narrowed glass capillary, and subsequent thermally induced reversal to spherical morphology. Scale bar 600 μm.

Measurement of DBCC crystal density by pycnometry (1.116 g·cm^{-3}) allows for the calculation of shell thickness. This is a simple geometric problem based on mass, and therefore volume, of DBCC present in a dodecane droplet of the specified size. For a 220 μm droplet of dodecane, the shell thickness would be ~2.52 μm if we assume a solid crystalline shell. Alternatively, for improved accuracy we can consider the packing density of high aspect ratio rods on the surface of a sphere (63%),[50,51] which gives an estimated thickness of ~4.05 μm. To calculate the shell thickness, semi-quantitatively, a confocal image of 220 μm capsules in reflectance mode with the focusing plane set at the center of the capsule, was thresholded (S11b) and the shell thickness was

measured using grey value intensity plots over 62 positions (5.72 ± 1.56 μm) and also manually over 149 positions (4.81 ± 1.21 μm) (S11c-d and S11a) over multiple capsules. Both methods reveal shell thickness above the predicted thickness, but this is to be expected due to focal depth artifacts from the confocal image. With this in mind, the predicted and measured values are in good agreement.

As mentioned previously, the crystal jammed nature of the bulk organogels led to crystal jammed structures stabilizing the dodecane droplets by needle-like crystals interlocking at the droplet surface. Similarly to Pickering stabilized of emulsion droplets, the crystal jamming effect here can be used to mold droplets into a non-spherical shape.[32] It was hypothesized that using a thermal transition, akin to the bulk organogels, would allow for reshaping of the capsules in geometric confinement. To test this theory a capsule captured in a capillary with a narrowing diameter was prepared. The capsule was first gently heated until a transition from crystalline to transparent oil was observed, as a result of crystal dissolution. The heated, transparent drop was moved to a narrower section of capillary and allowed to cool and reform the crystalline shell. The resulting reshaped drop had a "spherocylindrical" shape which was physically trapped and maintained its shape when moved back into the wider section of capillary (Figure 3d; see Video V2 in the SI). This demonstrates the ability to reshape capsules using a thermal transition to produce anisotropic capsules. The jammed, interlocked shell structure, prevents relaxation to a spherical capsule shape.

Given the large size of capsules produced by microfluidics, and potential complexities arising for commercial scale up, a simplified batch synthesis protocol using an equivalent binary dispersed phase was developed with the aim of producing microcapsules in the 10-50 μm range (see experimental section). A size analysis by light microscopy on 1000 particles revealed an average particle diameter of 9.09 ± 6.00 μm (Figure 4a and S12). The more translucent appearance of the

capsules is a direct result of the shell thickness reduction brought about by the volume:surface area relationship of spheres of decreasing size (Figure 4a). Smaller droplets result in a lower mass of DBCC per droplet, relative to surface area. Predicted shell thickness for these are ~190-370 nm for capsules between 10-20 µm. In this case, to get full coverage, a higher number of smaller crystals would be required. Looking at SEM comparisons between large and small (S14) capsules, it can be seen that the crystals are smaller in size on smaller capsules. Importantly, this also supports the surface nucleation theory proposed from Video V1 and illustrated in Video V3.

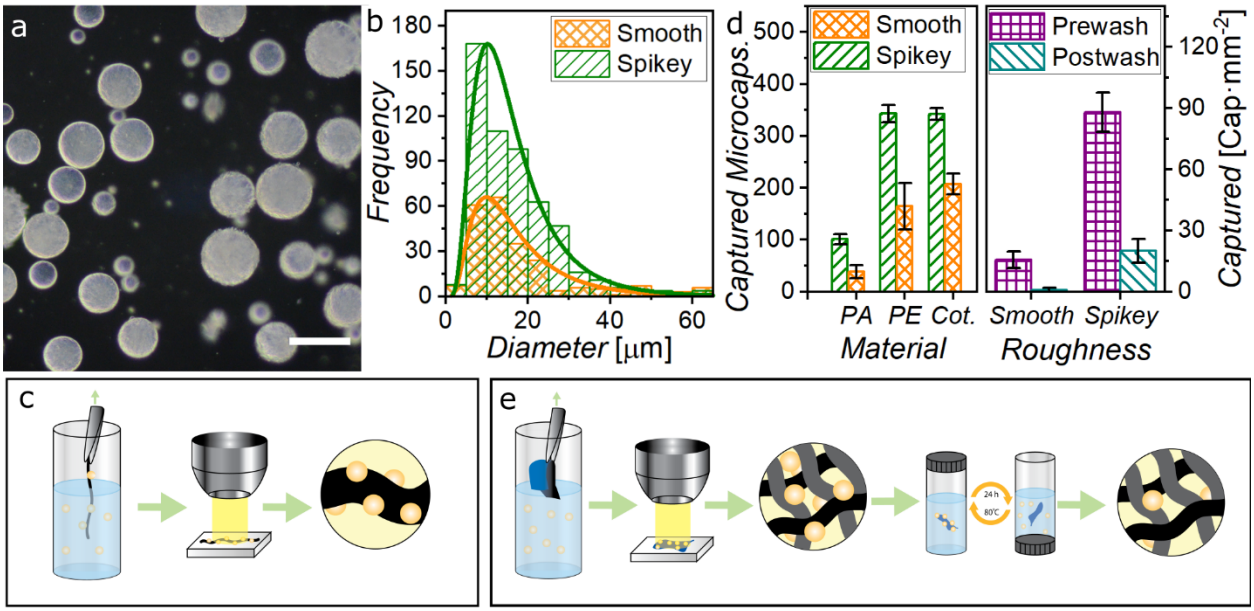

Figure 4. *(a)* Dark-field light microscopy of batch synthesized DBCC spikey capsules. Scale bar = 30 μm *(b)* Histograms of batch synthesis capsule sizes for smooth (cross diag.: coral) and spikey (diag. up: green) microcapsules *(c)* Schematic of fiber dip adhesion test *(d)* Column plots of fiber adhesion of smooth (cross diag.: coral) and spikey (diag. up: green). Also shown, adhesion pre (diag. down: teal) and post-wash (cross normal: purple) column plots of smooth and spikey capsules on cotton squares *(e)* Schematic of cotton square adhesion-wash test.

These smaller particles are applicable to the personal and household care industry as a non-polymeric encapsulation technique for oil soluble active ingredients, such as fragrances. It was proposed that the spikey shell of the microcapsules could provide improved adhesion to fibrous materials found in clothing. An analogy would be the way spikey pollen particles adhere to the legs of bees. To test this hypothesis batches of small spikey particles (16.65 μm ± 10.48) and equivalent smooth poly(urea) capsules (17.68 μm ± 13.11) were prepared (Figure 4b and S13-S15) for adhesion studies on Nylon, polyester and cotton fibers (S16).

In the first test, single fibers of polyamide, polyester and cotton were dipped into 1 wt.% dispersions of the capsules. The fibers were allowed to dry and the number of captured microcapsules were counted by light microscopy (Figure 4c). It was found that spikey capsules adhere at approximately twice the frequency of smooth capsules (2.6x polyamide, 2.0x polyester, 1.7x cotton- Figure 4d). In a second test, 100 mm^2 squares of cotton fabric were dipped in 1 wt.% dispersions of microcapsules and subsequently dried and capture frequencies were counted. Following this, the same cotton squares were washed in soap solution and tumbled overnight at 40 ^oC to simulate a laundry wash, followed by recounting of the retained capsules (Figure 4e). It was shown that the capsule retention rate of spikey capsules was higher (22.81 %) than that of smooth capsules (5.55 %), retaining 4.10x more particles (Figure 4d). Tests are illustrated through supplementary Figure S16 and S17.

The mechanism that accounts for the difference in adhesion could be attributed to different phenomenon including dewetting,[52] capillary pressure,[53] physical frictional adhesion from spikes catching on fiber textures and particle rolling, to name a few. [54] There have been countless studies looking at the influence of particle shape and roughness on adhesion.[55–58] In traditional particle physics, it is seen that a smooth sphere will have a higher area of contact than a homogenously

rough particle.[59] What is not traditionally accounted for is surface heterogeneity of both the particle and the surface.[60] It is proposed herein that perhaps the micron roughness of spikey particles could have favorable interaction with the surface heterogeneity of a non-ideal surface, thus increasing the surface area points of contact and increasing adhesive force through capillary under pressure. Additionally, another consideration to make is the shell structure in these microcapsules. The cage like structure stabilizing the droplet is highly porous and as a result the dodecane could wet to surfaces, increasing adhesive behavior. This seems a more credible explanation for the enhanced adhesion in these spikey capsules (Figure 5a-b).

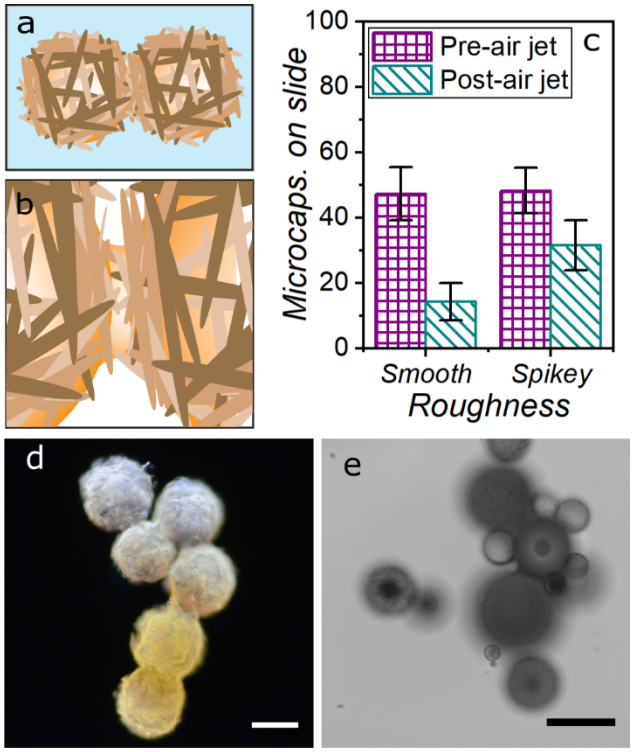

Figure 5. *(a-b)* Schematic of wetting between spikey capsules in close contact *(c)* Column chart showing capsules adhered to a glass slide pre (cross normal: purple) and post-air flow (diag. down: teal) *(d)* Dark-field microscopy of microfluidic microcapsules showing inter-capsule wetting. Scale bar = 100 μm *(e)* inverted light microscopy of wetting at the interface of spikey capsules and a glass microscope slide. Scale bar = 50 μm.

To test this, a combined dispersion of smooth and spikey capsules (1 wt.% of each) was cast onto a glass slide. The slide was dried and the number of adhered capsules of each type was counted. The glass slide was then subjected to a sustained jet of air to dry and remove capsules adhered by traditional capillary interactions with thin water films at the substrate-particle interface. Following counting of the remaining adhered microcapsules, it was found that there had been a 33.3 % loss of spikey capsules and a 68.8 % loss of smooth capsules. The results of this are also shown in Figure 5c.

A close analysis of capsules in close contact, by dark-field microscopy revealed bridging between particles (Figure 5d). The interface between spikey capsules and a glass substrate was also observed with an inverted microscope focused on the plane of the glass slides upper surface. This revealed dark contact patches where the wetting of dodecane through the capsule shell onto the glass substrate causes a refractive index difference (Figure 5e). Overall, this would indicate that the improved adhesion of spikey capsules over smooth capsules was a result of wetting from the capsule core solvent.

CONCLUSIONS

To conclude, this work shows the synthesis of microcapsules which are stabilized by an interlocked shell of small needle-like crystals. The use of a dual-solvent system allowed for crystal nucleation and growth from the dispersed phase at the emulsion droplet interface by evaporation of a volatile component. This 2-solvent system allowed for size prediction and control when capsules were generated by microfluidics. It was shown that the resulting capsules' shape could be manipulated by exploitation of the thermally dependent crystal solubility in the encapsulated dodecane. The unique jamming properties of the interlocking crystals making the shell, helped to

facilitate the retention of new geometries. Scale up of the capsule fabrication to a batch process using a conventional blender was shown to be possible, attaining microcapsules of a diameter applicable to commercial applications. It was observed that these small spikey capsules showed improved fiber adhesive properties compared to smooth equivalents. We postulated this to be a result of surface wetting from the solvent in the capsule core through the porous shell structure. It is our vision that capsules of this type are an alternative to polymer microcapsules, with great flexibility in choice of the molecular building blocks needed for crystal formation.

ASSOCIATED CONTENT

Supporting Information

The following files are available free of charge.

Supporting text, NMR, IR, DSC and Crystallographic data for the characterization of DBCC. Additional experimental details for construction of microfluidic devices. Additional microscopy of large and small capsules. Roughness and wall thickness measurements. – (PDF)

Supporting Video V1, microscope recording of microcapsule formation – (MPEG4)

Supporting Video V2, microscope recording of reversible capsule shape change – (MPEG4)

Supporting Video V3, animation illustrating the capsule formation process – (AVI)

Crystallographic data for DBCC – (CIF)

AUTHOR INFORMATION

Corresponding Author

*Stefan A. F. Bon, Department of Chemistry, University of Warwick, Gibbet Hill Road, Coventry, CV4 7AL, United Kingdom. E-Mail: s.bon@warwick.ac.uk

Present Addresses

†Samuel R. Wilson-Whitford, Department of Chemical and Biomolecular Engineering, Lehigh University, 19 Memorial Drive W., Bethlehem, Pennsylvania, 18015, USA.

§Brooke W. Longbottom, Department of Chemistry, University of Cambridge, Lensfied Road, Cambridge, CB2 1EW, United Kingdom

Author Contributions

The manuscript was written through contributions of all authors. All authors have given approval to the final version of the manuscript.

Notes

[CCDC 2009518 contains the supplementary crystallographic data for this paper. These data can be obtained free of charge from The Cambridge Crystallographic Data Centre via www.ccdc.cam.ac.uk/data_request/cif.]

ABBREVIATIONS

DBCC, decane-1,10-bis(cyclohexyl carbamate); DSC, Differential Scanning Calorimetry; PVA, polyvinyl alcohol; DCM, dichloromethane; SEM, Scanning Electron Microscopy; NMR, Nuclear Magnetic Resonance; HRMS, High Resolution Mass Spectrometry.

REFERENCES

(1) Ammala, A. Biodegradable Polymers as Encapsulation Materials for Cosmetics and Personal Care Markets. *Int. J. Cosmet. Sci.* **2013**, *35* (2), 113–124.

(2) Tekin, R.; Bac, N.; Erdogmus, H. Microencapsulation of Fragrance and Natural Volatile Oils for Application in Cosmetics, and Household Cleaning Products. *Macromol. Symp.* **2013**, *333* (1), 35–40.

(3) Biary, B.; Lheureux, E. Microcapsules with an Aqueous Core Containing at Least One Water-Soluble Cosmetic or Dermatological Active Principle and Cosmetic or Dermatological Compositions Containing Them. US6531160B2, 2000.

(4) Jungmann, N.; Lersch, P.; Schick, U.; Schiemann, Y.; Weitemeyer, C. Cosmetic Preparations Comprising Active Ingredients in Microcapsules. US20040161438A1, 2003.

(5) Bala, K.; Vasudevan, P. Polymeric Microcapsules for Drug Delivery. *J. Macromol. Sci. Part A - Chem.* **1981**, *16* (4), 819–827.

(6) Saenz del Burgo, L.; Ciriza, J.; Espona-Noguera, A.; Illa, X.; Cabruja, E.; Orive, G.; Hernández, R. M.; Villa, R.; Pedraz, J. L.; Alvarez, M. 3D Printed Porous Polyamide Macrocapsule Combined with Alginate Microcapsules for Safer Cell-Based Therapies. *Sci. Rep.* **2018**, *8* (1), 8512.

(7) Kroneková, Z.; Pelach, M.; Mazancová, P.; Uhelská, L.; Treľová, D.; Rázga, F.; Némethová, V.; Szalai, S.; Chorvát, D.; McGarrigle, J. J.; Omami, M.; Isa, D.; Ghani, S.; Majková, E.; Oberholzer, J.; Raus, V.; Šiffalovič, P.; Lacík, I. Structural Changes in Alginate-Based Microspheres Exposed to in Vivo Environment as Revealed by Confocal Raman Microscopy. *Sci. Rep.* **2018**, *8* (1), 1637.

(8) Chen, T.; Colver, P. J.; Bon, S. A. F. Organic-Inorganic Hybrid Hollow Spheres Prepared from TiO 2-Stabilized Pickering Emulsion Polymerization. *Adv. Mater.* **2007**, *19* (17), 2286–2289.

(9) Li, J.; Hitchcock, A. P.; Stöver, H. D. H.; Shirley, I. A New Approach to Studying Microcapsule Wall Growth Mechanisms. *Macromolecules* **2009**, *42* (7), 2428–2432.

(10) Niederholtmeyer, H.; Chaggan, C.; Devaraj, N. K. Communication and Quorum Sensing in Non-Living Mimics of Eukaryotic Cells. *Nat. Commun.* **2018**, *9* (1), 5027.

(11) Dou, H.; Li, M.; Qiao, Y.; Harniman, R.; Li, X.; Boott, C. E.; Mann, S.; Manners, I. Higher-Order Assembly of Crystalline Cylindrical Micelles into Membrane-Extendable Colloidosomes. *Nat. Commun.* **2017**, *8* (1), 426.

(12) Zakharchenko, S.; Ionov, L. Anisotropic Liquid Microcapsules from Biomimetic Self-Folding Polymer Films. *ACS Appl. Mater. Interfaces* **2015**, *7* (23), 12367–12372.

(13) Wang, H.; Zhao, Z.; Liu, Y.; Shao, C.; Bian, F.; Zhao, Y. Biomimetic Enzyme Cascade Reaction System in Microfluidic Electrospray Microcapsules. *Sci. Adv.* **2018**, *4* (6), eaat2816.

(14) Chang, T. M. S. Semipermeable Microcapsules. *Science* **1964**, *146* (3643), 524–525.

(15) Fessi, H.; Puisieux, F.; Devissaguet, J.-P. Process for Preparing a Colloidal and Disperse System in the Shape of Nanocapsules. EP0274961A1, 1986.

(16) Fessi, H.; Puisieux, F.; Devissaguet, J.-P.; Ammoury, N.; Benita, S. Nanocapsule Formation by Interfacial Polymer Deposition Following Solvent Displacement. *Int. J. Pharm.* **1989**, *55* (1), R1–R4.

(17) Yadav, S. K.; Khilar, K. C.; Suresh, A. K. Release Rates from Semi-Crystalline Polymer Microscapsules Formed by Interfacial Polycondensation. *J. Memb. Sci.* **1997**, *125*, 213–218.

(18) Wang, W.; Qi, H.; Zhou, T.; Mei, S.; Han, L.; Higuchi, T.; Jinnai, H.; Li, C. Y. Highly Robust Crystalsome via Directed Polymer Crystallization at Curved Liquid/Liquid Interface. *Nat. Commun.* **2016**, *7*, 10599.

(19) Qi, H.; Zhou, H.; Tang, Q.; Lee, J. Y.; Fan, Z.; Kim, S.; Staub, M. C.; Zhou, T.; Mei, S.; Han, L.; Pochan, D. J.; Cheng, H.; Hu, W.; Li, C. Y. Block Copolymer Crystalsomes with an Ultrathin Shell to Extend Blood Circulation Time. *Nat. Commun.* **2018**, *9*, 3005.

(20) Velev, O. D.; Furusawa, K.; Nagayama, K. Assembly of Latex Particles by Using Emulsion Droplets as Templates. 1. Microstructured Hollow Spheres. *Langmuir* **1996**, *12* (10), 2374–2384.

(21) Dinsmore, A. D.; Hsu, M. F.; Nikolaides, M. G.; Marquez, M.; Bausch, A. R.; Weitz, D. A. Colloidosomes: Selectively Permeable Capsules Composed of Colloidal Particles. *Science* **2002**, *298* (5595), 1006–1009.

(22) Ramsden, W.; Oxon, M. D. Separation of Solids in the Surface-Layers of Solutions and Suspensions. *Proc. R. Soc. Lond.* **1904**, *72*, 156–164.

(23) Pickering, S. U. CXCVI.—Emulsions. *J. Chem. Soc., Trans.* **1907**, *91* (0), 2001–2021.

(24) Ballard, N.; Law, A. D.; Bon, S. A. F. Colloidal Particles at Fluid Interfaces: Behaviour of Isolated Particles. *Soft Matter* **2019**, *15* (6), 1186–1199.

(25) Huck, W. T. S.; Tien, J.; Whitesides, G. M. Three-Dimensional Mesoscale Self-Assembly. *J. Am. Chem. Soc.* **1998**, *120* (10), 8267–8268.

(26) Bausch, A. R.; Bowick, M. J.; Cacciuto, A.; Dinsmore, A. D.; Hsu, M. F.; Nelson, D. R.; Nikolaides, M. G.; Travesset, A.; Weitz, D. A. Grain Boundary Scars and Spherical Crystallography. *Science* **2003**, *299*, 1716–1718.

(27) Lipowsky, P.; Bowick, M. J.; Meinke, J. H.; Nelson, D. R.; Bausch, A. R. Direct Visualization of Dislocation Dynamics in Grain-Boundary Scars. *Nat. Mater.* **2005**, *4*, 407–411.

(28) Bon, S. A. F.; Chen, T. Pickering Stabilization as a Tool in the Fabrication of Complex Nanopatterned Silica Microcapsules. *Langmuir* **2007**, *23* (19), 9527–9530.

(29) Bon, S. A. F.; Cauvin, S.; Colver, P. J. Colloidosomes as Micron-Sized Polymerisation Vessels to Create Supracolloidal Interpenetrating Polymer Network Reinforced Capsules. *Soft Matter* **2007**, *3* (2), 194–199.

(30) Noble, P. F.; Cayre, O. J.; Alargova, R. G.; Velev, O. D.; Paunov, V. N. Fabrication of "Hairy" Colloidosomes with Shells of Polymeric Microrods. *J. Am. Chem. Soc.* **2004**, *126* (26), 8092–8093.

(31) Subramaniam, A. B.; Abkarian, M.; Stone, H. A. Controlled Assembly of Jammed Colloidal Shells on Fluid Droplets. *Nat. Mater.* **2005**, *4*, 553–556.

(32) Bon, S. A. F.; Mookhoek, S. D.; Colver, P. J.; Fischer, H. R.; van der Zwaag, S. Route to Stable Non-Spherical Emulsion Droplets. *Eur. Polym. J.* **2007**, *43* (11), 4839–4842.

(33) Alargova, R. G.; Warhadpande, D. S.; Paunov, V. N.; Velev, O. D. Foam Superstabilization by Polymer Microrods. *Langmuir* **2004**, *20* (24), 10371–10374.

(34) Alargova, R. G.; Paunov, V. N.; Velev, O. D. Formation of Polymer Microrods in Shear Flow by Emulsification– Solvent Attrition Mechanism. *Langmuir* **2006**, *22*, 765–774.

(35) Paunov, V. N.; Cayre, O. J.; Noble, P. F.; Stoyanov, S. D.; Velikov, K. P.; Golding, M. Emulsions Stabilised by Food Colloid Particles: Role of Particle Adsorption and Wettability at the Liquid Interface. *J. Colloid Interface Sci.* **2007**, *312* (2), 381–389.

(36) Zhou, W.; Cao, J.; Liu, W.; Stoyanov, S. How Rigid Rods Self-Assemble at Curved Surfaces. *Angew. Chemie Int. Ed.* **2009**, *48* (2), 378–381.

(37) Wang, X.; Zhou, W.; Cao, J.; Liu, W.; Zhu, S. Preparation of Core–Shell CaCO3 Capsules via Pickering Emulsion Templates. *J. Colloid Interface Sci.* **2012**, *372* (1), 24–31.

(38) Nie, Z.; Jai, I. P.; Li, W.; Bon, S. A. F.; Kumacheva, E. An "inside-out" Microfluidic Approach to Monodisperse Emulsions Stabilized by Solid Particles. *J. Am. Chem. Soc.* **2008**, *130* (49), 16508–16509.

(39) Eslami, F.; Elliott, J. A. W. Role of Precipitating Solute Curvature on Microdrops and Nanodrops during Concentrating Processes: The Nonideal Ostwald-Freundlich Equation. *J. Phys. Chem. B* **2014**, *118* (50), 14675–14686.

(40) Leng, J.; Salmon, J.-B. Microfluidic Crystallization. *Lab Chip* **2009**, *9* (1), 24–34.

(41) Spiegel, B.; Käfer, A.; Kind, M. Crystallization Behavior and Nucleation Kinetics of Organic Melt Droplets in a Microfluidic Device. *Cryst. Growth Des.* **2018**, *18* (6), 3307–3316.

(42) Wang, J.; Zhang, J.; Han, J. Synthesis of Crystals and Particles by Crystallization and Polymerization in Droplet-Based Microfluidic Devices. *Front. Chem. Eng. China* **2010**, *4* (1), 26–36.

(43) Jaggers, R. W.; Chen, R.; Bon, S. A. F. Control of Vesicle Membrane Permeability with Catalytic Particles. *Mater. Horiz.* **2016**, *3* (1), 41–46.

(44) Sugimoto, T.; Moria, T.; Mano, J.; Mutoh, T. A.; Shiinoki, Y.; Matsumura, Y. Effects of Fat Crystallization on the Behavior of Proteins and Lipids at Oil Droplet Surfaces. *JAOCS, J. Am. Oil Chem. Soc.* **2001**, *78* (2), 183–188.

(45) Herhold, A. B.; Ertas, D.; Levine, A. J.; King Jr., H. E. Impurity Mediated Nucleation in Hexadecane-in-Water Emulsions. *Phys. Rev. E* **1999**, *59*, 6946.

(46) Utada, A. S.; Fernandez-Nieves, A.; Stone, H. A.; Weitz, D. A. Dripping to Jetting Transitions in Coflowing Liquid Streams. *Phys. Rev. Lett.* **2007**, *99*, 094502.

(47) Umbanhowar, P. B.; Prasad, V.; Weitz, D. A. Monodisperse Emulsion Generation via Drop Break off in a Coflowing Stream. *Langmuir* **2000**, *16*, 347–351.

(48) Clanet, C.; Lasheras, J. C. Transition from Dripping to Jetting. *J. Fluid Mech.* **1999**, *383*, 307–326.

(49) Thorne, M. F.; Simkovic, F.; Slater, A. G. Production of Monodisperse Polyurea Microcapsules Using Microfluidics. *Sci. Rep.* **2019**, *9* (1), 17983.

(50) Kyrylyuk, A. V.; Wouterse, A.; Philipse, A. P. Random Packings Of Rod-Sphere Mixtures Simulated By Mechanical Contraction. *AIP Conf. Proc.* **2009**, *1145*, 211–214.

(51) Smallenburg, F.; Lowen, H. Close Packing of Rods on Spherical Surfaces. *J. Chem. Phys.* **2016**, *144*, 164903.

(52) Weon, B. M.; Ho Je, J. Capillary Force Repels Coffee-Ring Effect. *Phys. Rev. E* **2010**, *82*, 015305.

(53) Kralchevsky, P. A.; Nagayama, K. Capillary Forces between Colloidal Particles. *Langmuir* **1994**, *10* (1), 23–36.

(54) Cross, R. Effects of Surface Roughness on Rolling Friction. *Eur. J. Phys.* **2015**, *36* (6), 065029.

(55) Götzinger, M.; Peukert, W. Particle Adhesion Force Distributions on Rough Surfaces. *Langmuir* **2004**, *20* (13), 5298–5303.

(56) Li, Q.; Pohrt, R.; Popov, V. L. Adhesive Strength of Contacts of Rough Spheres. *Front. Mech. Eng.* **2019**, *5*, 1–9.

(57) Chatterjee, N.; Flury, M. Effect of Particle Shape on Capillary Forces Acting on Particles at the Air–Water Interface. *Langmuir* **2013**, *29* (25), 7903–7911.

(58) van Zwol, P.; Palasantzas, G.; De Hosson, J. M. T. Influence of Roughness on Capillary Forces between Hydrophilic Surfaces. *Phys. Rev. E* **2008**, *78*, 031606.

(59) Corn, M. The Adhesion of Solid Particles to Solid Surfaces, I. a Review. *J. Air Pollut. Control Assoc.* **1961**, *11* (11), 523–528.

(60) Butt, H.-J. Capillary Forces: Influence of Roughness and Heterogeneity. *Langmuir* **2008**, *24* (9), 4715–4721.

TABLE OF CONTENTS